Supplementary Information (SI) for Journal of Materials Chemistry A.

Supporting Information

Pebax Mixed Matrix Membranes Based on Novel HOF/MOF Nanofiller with Simultaneous Improvement in CO_2 Permeability and CO_2/N_2 Selectivity

Zikang Qin[a], Jing Wei[b], Wen Hou[c], Zhuo Chen[c], Min Deng[b], Lu Yao[a,d,e], Dengrong Sun[a,d,e], Lin Yang[a,d,e], Wenju Jiang[a,d,e], Junfeng Zheng[a,d,e], Yutian Li[f], Qiang Jing[g,h]*, and Zhongde Dai[a,d,e]*

[a]College of Carbon Neutrality Future Technology, Sichuan University, Chengdu 610065, China

[b]College of Architecture and Environment, Sichuan University, Chengdu 610065, China

[c]DongFang Boiler Co.,Ltd., Zigong 643001, China

[d]National Engineering Research Centre for Flue Gas Desulfurization, Chengdu 610065, China

[e]Carbon Neutral Technology Innovation Center of Sichuan, Chengdu 610065, China

[f]Petrochina planning & engineering Institute

[g]Shenzhen Shenshan Special Cooperation Zone China Resources Power Co., Ltd, Shenzhen 518066, China

[h]Guangdong Run Carbon Technology Co.,Ltd., Shenzhen 518000, China

*Corresponding author:

Qiang Jing, E-mail: njjq360@163.com

Zhongde Dai, E-mail: zhongde.dai@scu.edu.cn

Table of contents

1. Single-gas permeation experiment

The permeation properties of three series of MMMs for pure CO_2, CH_4, and N_2 were tested using a single-gas permeation setup as shown in **Fig. S1**. The operation temperature range was 25-45 °C, the pressure was varied from 2-6 bar, and evacuation was taken upstream and downstream of the MMMs before each test.

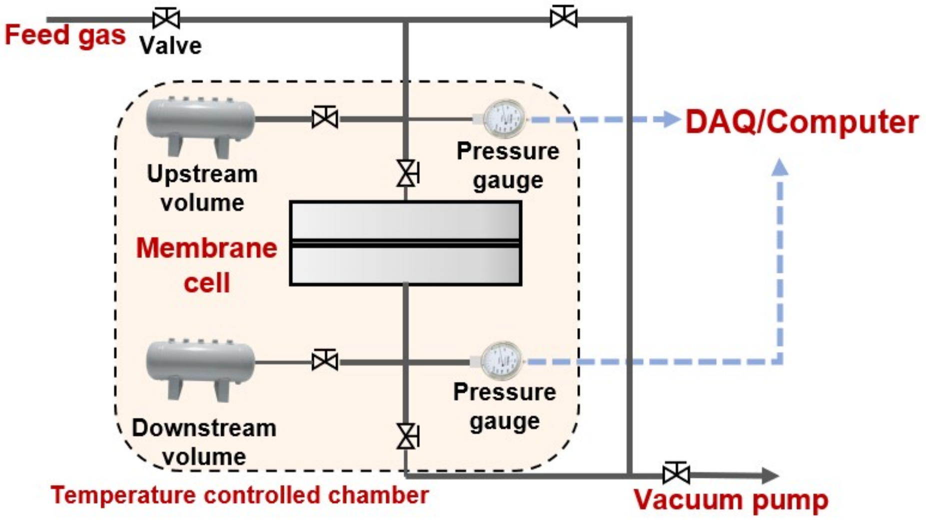

Fig. S1. Schematic diagram of single-gas permeation setup

The permeability (P) of the MMM was calculated from the slope of the pressure-time curve (dp/dt) using **equation (1)**.

$$P = \frac{VL}{ATRP_0}\left[\frac{dp(t)}{dt_s} - \frac{dp(t)}{dt_{leak}}\right] \times 10^{10} \qquad (1)$$

where, P is the gas permeability, Barrer; V is the downstream volume, cm^3; L is the membrane thickness, cm; P_0 is the transmembrane pressure difference, cmHg; A is the effective gas transport area, cm^2; R is the gas constant, 0.278 $cmHgcm^3cm^{-3}(STP)K^{-1}$; T is the test temperature, K; $\frac{dp(t)}{dt_s}$ and $\frac{dp(t)}{dt_{leak}}$ are the downstream pressure rise rates with and without air inlet, $cmHg{\cdot}s^{-1}$. The ideal selectivity $\alpha^*_{x/y}$ for MMMs is calculated as shown in **equation (2)**:

$$\alpha^{*}_{x/y} = \frac{P_x}{P_y} \qquad (2)$$

Where, P_x and P_y are the permeability of the gas components x and y, respectively.

2. Magnified SEM images of Cu-MOF and Cu-MOF/HOF (15)

The magnified image of Cu-MOF after re-sonication is shown in **Fig. S2a**, which has a spherical morphology with a particle size of about 20 nm. In addition, for Cu-MOF/HOF (15), it also has a spherical star morphology, but with a smoother surface, as shown in **Fig. S2b**.

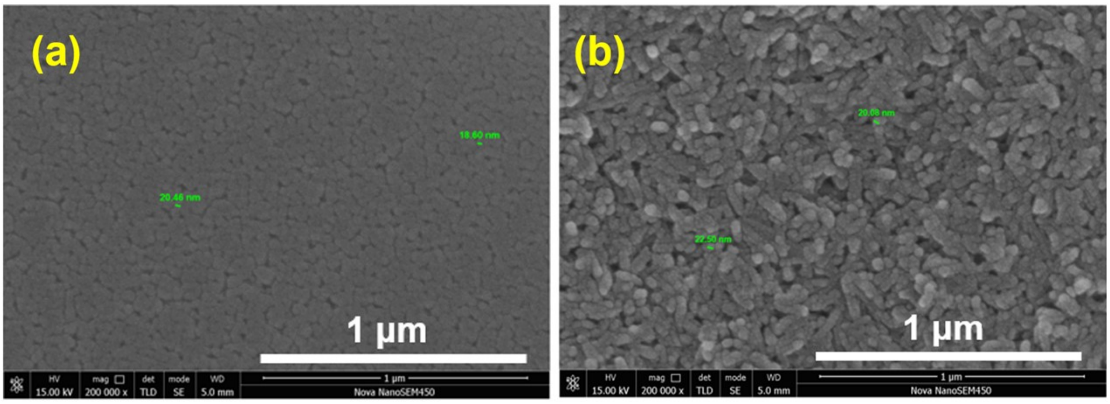

Fig. S2 Cu-MOF after re-sonication (a) and Cu-MOF/HOF after re-magnification (15) (b)

3. Magnified SEM image of Cu-MOF/HOF (10)

For Cu-MOF/HOF(10), the morphology transforms into a rod-like structure approximately 1 μm in length, as shown in **Fig. S3**.

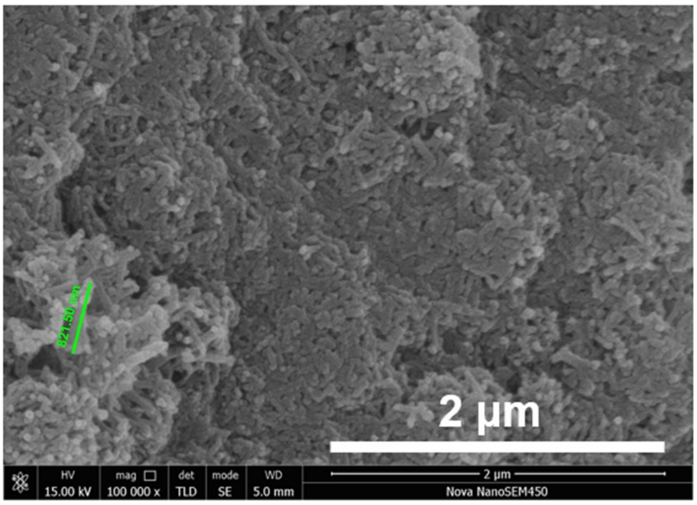

Fig. S3 Cu-MOF/HOF(10) with labeling

4. XRD results of HOF-21

The XRD results of the prepared HOF-21 are shown in **Fig. S4**, which are in perfect agreement with the standard card, indicating the successful preparation of HOF-21. Upon comparison, shortening the reaction time (4 days in most reports and 15 min in the present work) similarly allowed the synthesis of HOF-21 with a good structure [1, 2]。

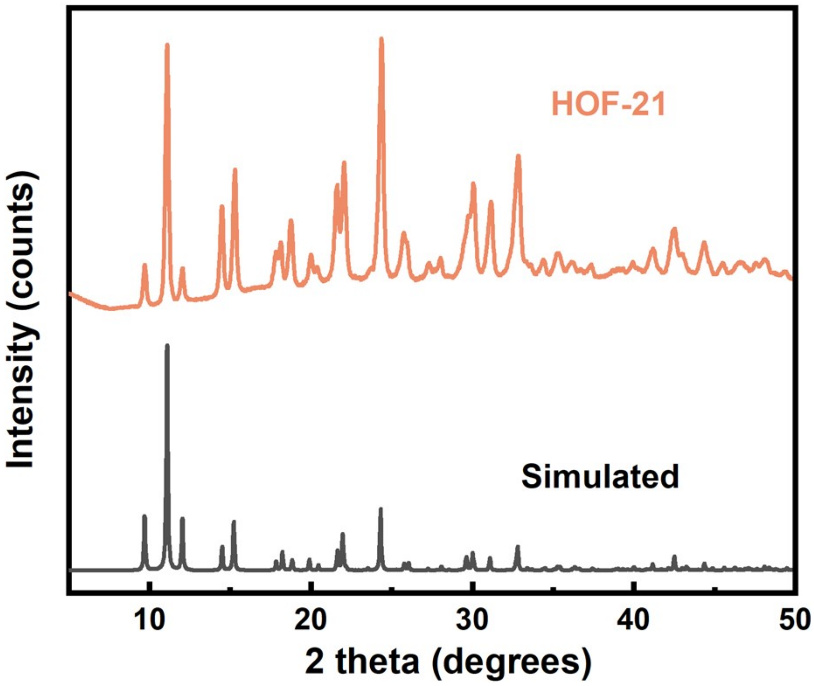

Fig. S4 XRD results of HOF-21

5. Magnified XRD comparison of four fillers

With the increase of HOF-21 reaction molar ratio, peaks belonging to HOF-21 appeared in the XRD results of Cu-MOF/HOF and were gradually obvious, as shown in **Fig. S5,** indicating that HOF-21 modified Cu-MOF successfully [3]。

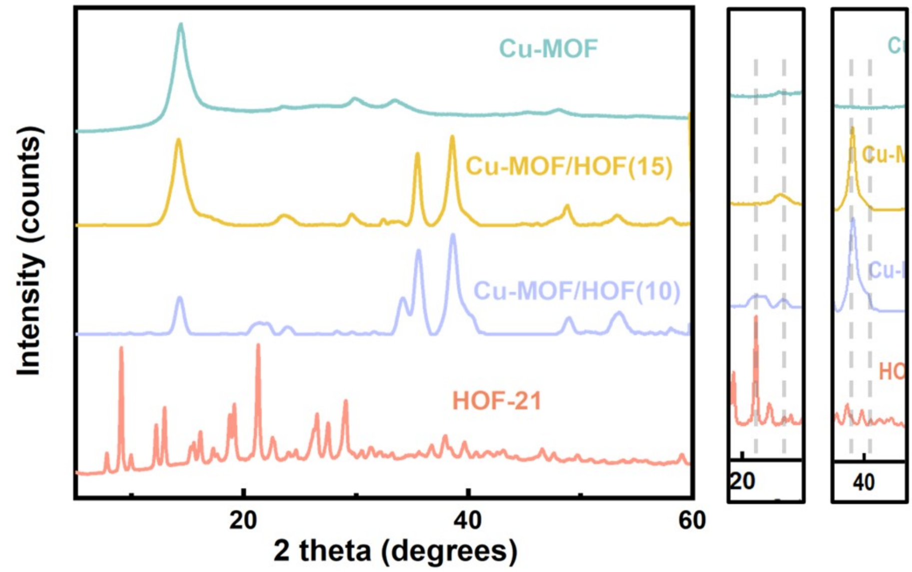

Fig. S5. Magnified XRD comparison of four fillers

6. DTG of four fillers

The DTG curves of four fillers are shown in **Fig. S6**. Both Cu-MOF/HOF(10) and Cu-MOF/HOF(15) exhibit the thermal weight loss characteristics of both HOF-21 and Cu-MOF, and as the molar ratio of adenine to $(NH_4)_2SiF_6$ increases, the characteristics of HOF-21 become increasingly pronounced. Notably, after modification with HOF-21, the DTG curve of Cu-MOF/HOF shifts to the right, indicating an improvement in thermal stability.

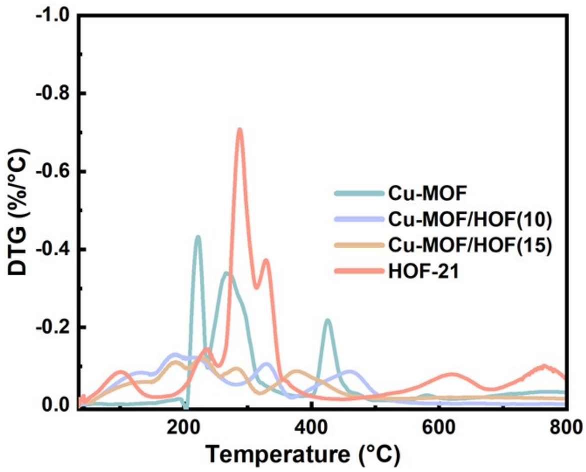

Fig. S6 DTG curves of four fillers

7. SEM images of Pebax-Cu-MOF 10 wt.% MMM

The surface and cross-section SEM images of Pebax-Cu-MOF 10 wt.% MMMs are shown in **Fig. S7**. At higher loadings, it can be observed that clear interfacial voids and filler agglomeration in the membrane surface and cross-section. In addition, in the cross-section SEM schematic, it can be observed that the longitudinal uniform distribution of spherical Cu-MOF is not enriched to one side, and the surface its distribution is relatively uniform in the longitudinal direction.

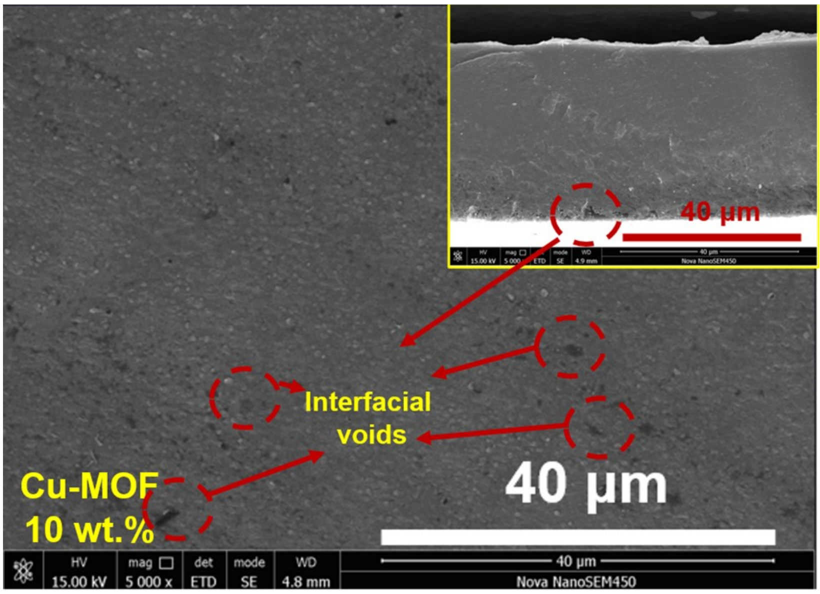

Fig. S7 Surface and cross-section (yellow box) SEM images of Pebax-Cu-MOF 10 wt.% MMM.

8. The EDS elemental distributions of MMMs

The EDS elemental distributions of Pebax-Cu-MOF/HOF(15) 3.5 wt.% and Pebax-Cu-MOF/HOF(10) 3.5 wt.% MMMs are shown in **Fig. S8**. Notably, Si is uniformly distributed along with Cu, indicating that Cu-MOF/HOF was successfully incorporated into Pebax with a uniform distribution.

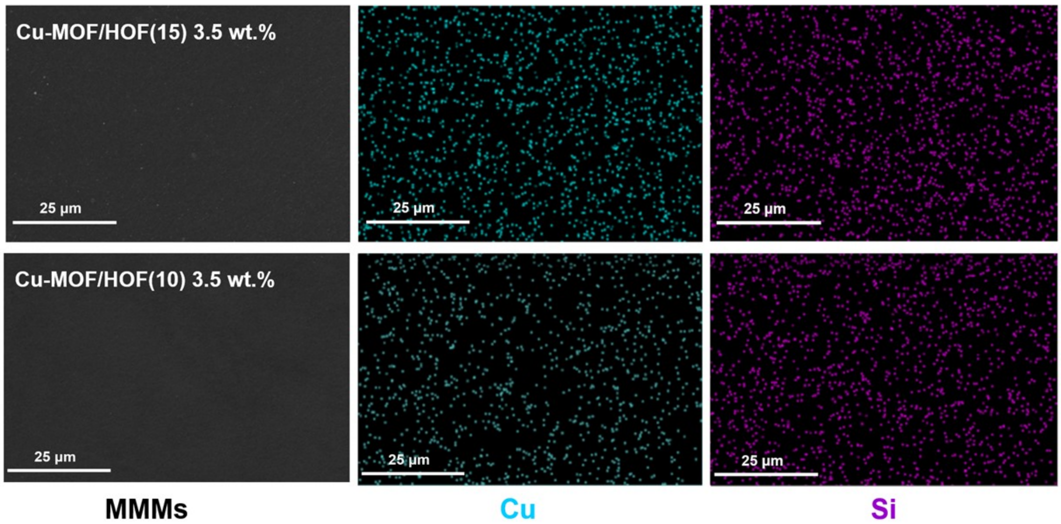

Fig. S8 The EDS elemental distributions of Pebax-Cu-MOF/HOF(15) 3.5 wt.% and Pebax-Cu-MOF/HOF(10) 3.5 wt.% MMMs

9. FTIR characterization of three series of MMMs

The magnified FTIR results of the three series of MMMs are shown in **Fig. S9**. After the introduction of Cu-MOF, Cu-MOF/HOF(15), and Cu-MOF/HOF(10), the appearance of peaks belonging to HMIM was observed in the range of 670-685 cm^{-1} for all MMMs, indicating the successful introduction of MOF.

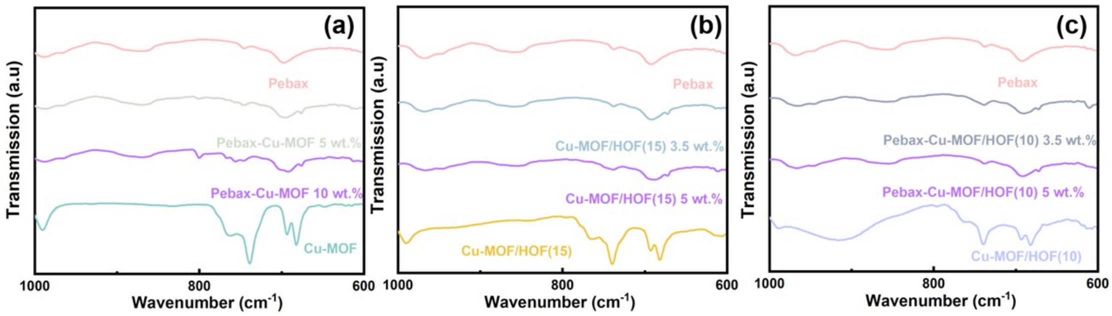

Fig. S9 FTIR characterization of MMMs (magnified), (a) Pebax-Cu-MOF MMMs; (b) Pebax-Cu-MOF/HOF(15) MMMs; (c) Pebax-Cu-MOF/HOF(10) MMMs

10. DTG of three series of MMMs

Fig. S10 presents the DTG results of three series of MMMs. After the introduction of fillers, the thermal decomposition process of MMMs was accelerated, and this tendency became more pronounced with increasing filler loading, which is consistent with the expected behavior.

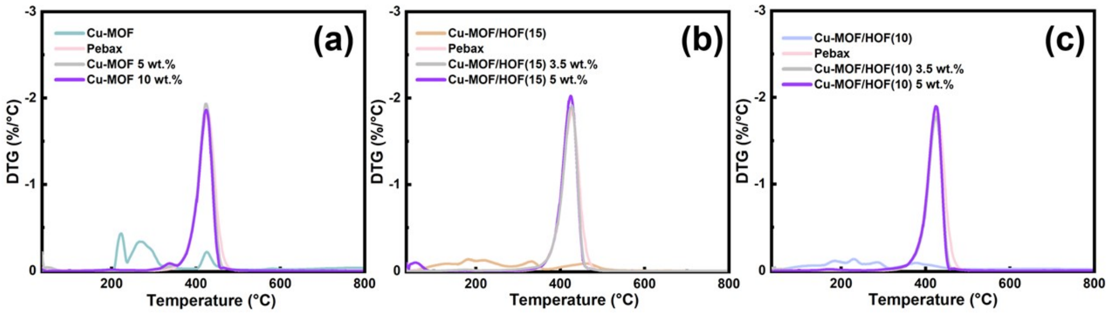

Fig. S10 DTG curves of three series of MMMs, Pebax-Cu-MOF MMMs (a), Pebax-Cu-MOF/HOF(15) MMMs (b), and Pebax-Cu-MOF/HOF(10) MMMs (c)

11. D-spacing of MMMs

The d-spacing of all MMMs was calculated by the Bragg equation and the results are shown in **Table S1**. The d-spacing of all MMMs is higher than that of pure Pebax, indicating that the introduction of MOF can break the original chain stacking of the polymer chains and increase the polymer chain mobility, thus facilitating the transport of gas molecules [4-6].

Table S1. d-spacing of MMMs

MMMs	Loading (wt.%)	d-spacing (Å)
Pebax	0	3.665
Pebax-Cu-MOF	5	3.719
Pebax-Cu-MOF	10	3.722
Pebax-Cu-MOF/HOF(15)	3.5	3.707
Pebax-Cu-MOF/HOF(15)	5	3.713
Pebax-Cu-MOF/HOF(10)	3.5	3.675
Pebax-Cu-MOF/HOF(10)	5	3.687

12. Mechanical properties of the MMMs

The tensile stress and elongation at break with the prepared MMMs are shown in **Fig. S11**. For Pebax, the maximum tensile stress and elongation at break were 11.08 MPa and 407.2%, respectively. However, after the introduction of the filler, the MMM became brittle due to incompatibilities between the polymer and the filler, which resulted in the maximum tensile stresses of Pebax-Cu-MOF/HOF (15) 3.5 wt.% Pebax-Cu-MOF 3.5 wt% MMM decreasing to 9.845 MPa and 8.116 MPa, and the elongation at break decreasing to 349.9% and 246.2%, respectively.

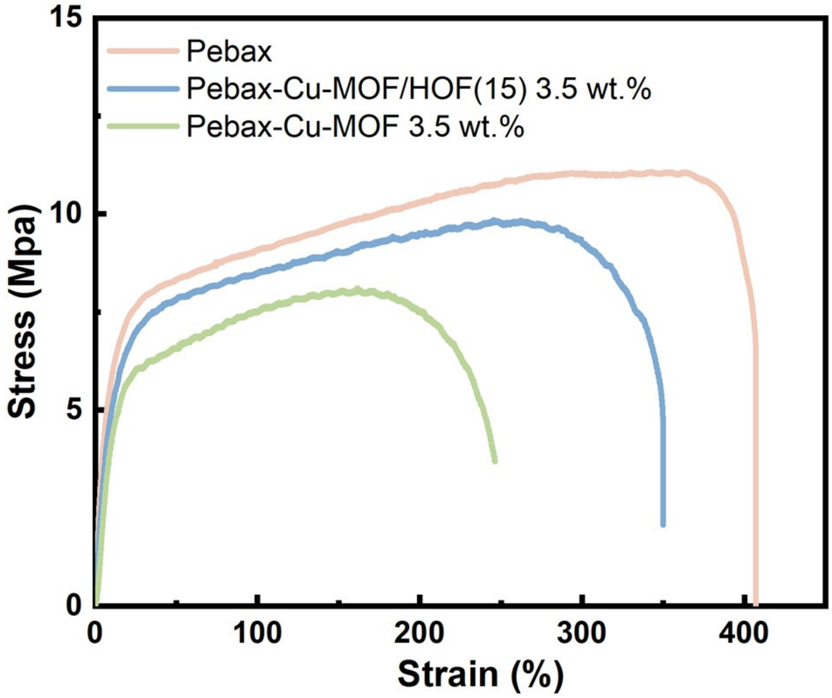

Fig. S11 Mechanical properties of the MMMs

13. CO_2/CH_4 separation performance of three series of MMMs

The CO_2/CH_4 separation performance of three series of MMMs with different filler loadings is shown in **Fig. S12**. Similar to the CO_2/N_2 separation performance, both CO_2 permeability and CO_2/CH_4 selectivity of the three series of MMMs initially increase and then decrease as the filler loading increases. Specifically, the P_{CO_2} of Pebax-Cu-MOF 5 wt.%, Pebax-Cu-MOF/HOF(15) 3.5 wt.%, and Pebax-Cu-MOF/HOF(10) 3.5 wt.% MMMs are 79.67 Barrer, 118.9 Barrer, and 98.84 Barrer, and $\alpha^*_{CO_2/CH_4}$ are 15.38, 17.13, and 14.0, respectively. However, with further elevation of MMMs loading, the P_{CO_2} and $\alpha^*_{CO_2/CH_4}$ of the three series of MMMs were reduced, with the Pebax-Cu-MOF 10 wt.%, the Pebax-Cu-MOF/HOF(15) 5 wt.% and Pebax-Cu-MOF/HOF(10) 5 wt.% MMMs had a P_{CO_2} of 73.68 Barrer, 96.53 Barrer, and a $\alpha^*_{CO_2/CH_4}$ of 14.83, 17.12, respectively, which were attributed to the fact that the MOFs were agglomerated at high loading, affecting their gas transfer channels. which affects the performance of its role as a gas mass transfer channel, however, for Pebax-Cu-MOF/HOF(10) 5 wt.% MMMs, it exhibits a decrease in P_{CO_2} (93.77 Barrer) and an increase in $\alpha^*_{CO_2/CH_4}$ (14.19), which may be related to the fact that the rod structure is more homogeneously filled at high loadings.

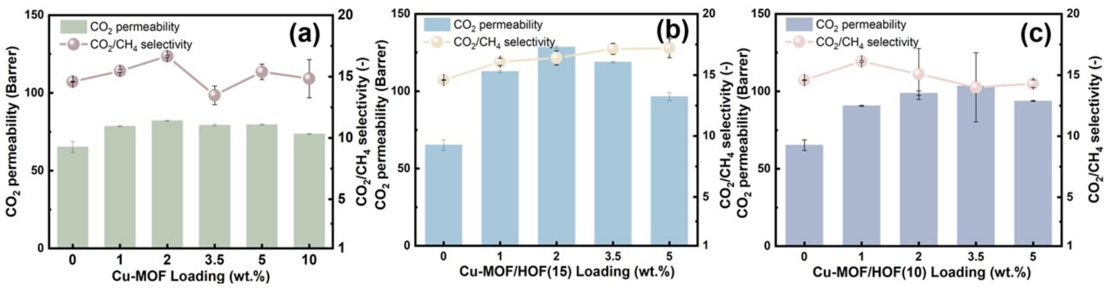

Fig. S12 CO_2/CH_4 separation performance of three series of MMMs, (a) Pebax-Cu-MOF MMMs; (b) Pebax-Cu-MOF/HOF(15) MMMs; (c) Pebax-Cu-MOF/HOF(10) MMMs

14. S_{CO_2/N_2} and D_{CO_2/N_2} of MMMs under different pressures

As pressure increases, the S_{CO_2/N_2} ratios of MMMs decrease, while the D_{CO_2/N_2} ratios increase as shown in **Fig. S13**. However, for Pebax-Cu-MOF/HOF (15) 3.5 wt.% MMM, when the pressure was increased from 2 bar to 6 bar, the CO_2/N_2 selectivity increased from 71.78 to 75.53. This upward trend is primarily attributed to changes in D_{CO_2/N_2}, which aligns with the plasticization resistance of MMMs and the influence of Cu-MOF/HOF.

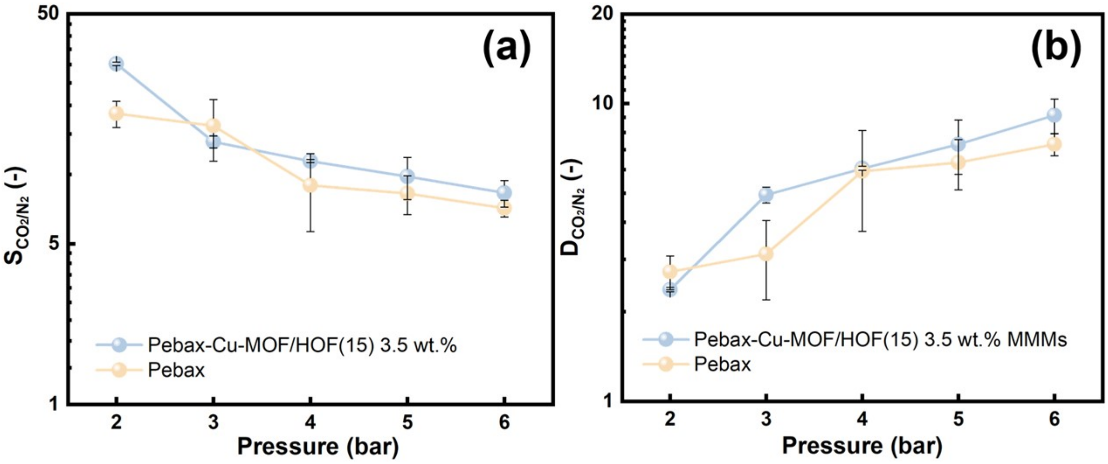

Fig. S13 S_{CO_2/N_2} (a) and D_{CO_2/N_2} (b) of MMMs

15. Effect of feed pressure

The $\alpha^*_{CO_2/CH_4}$ of Pebax and Pebax-Cu-MOF/HOF(15) 3.5 wt.% MMMs at 25 °C when the pressure was varied from 2 bar to 6 bar are shown in **Fig. S14**. The $\alpha^*_{CO_2/CH_4}$ of Pebax and Pebax-Cu-MOF/HOF (15) 3.5 wt.% MMMs fluctuated slightly with increasing pressure but remained essentially constant.

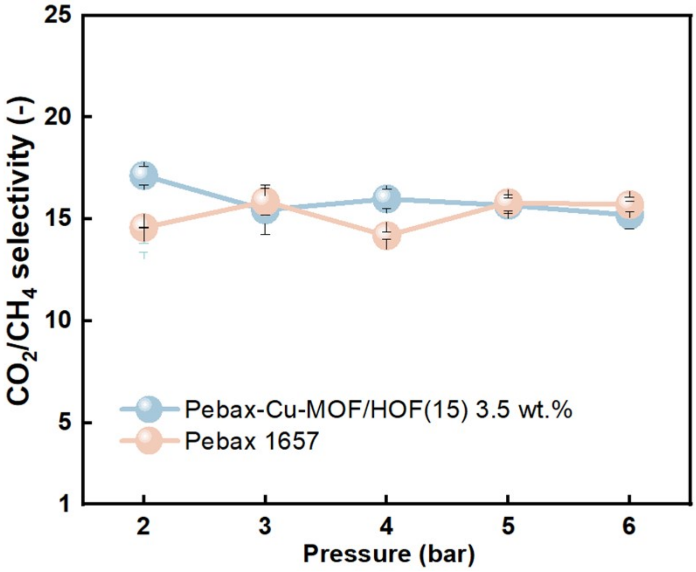

Fig. S14 $\alpha^*_{CO_2/CH_4}$ of Pebax and Pebax-Cu-MOF/HOF(15) 3.5 wt.% MMMs at 25 °C with different pressures.

16. Effect of temperature

The CO_2/CH_4 separation performance of Pebax and Pebax-Cu-MOF/HOF (15) 3.5 wt.% MMMs at 2 bar pressure and temperature increase from 25 °C to 45 °C is shown in **Fig. S15**. When the temperature rises from 25 ℃ to 45 ℃, the P_{CO_2} of Pebax-Cu-MOF/HOF(15) 3.5 wt.% and Pebax increased from 118.9 Barrer and 65.22 Barrer to 178.3 Barrer and 107.0 Barrer, respectively. Meanwhile, the $\alpha^*_{CO_2/CH_4}$ decreased from 17.13 and 14.58 to 11.54 and 8.910, respectively. The above phenomena can be attributed to increased temperature and accelerated gas diffusion, which results in increased permeability of both CO_2 and CH_4 and decreased $\alpha^*_{CO_2/CH_4}$, in addition to a more detailed discussion can be found in section 3.3.3 of the manuscript.

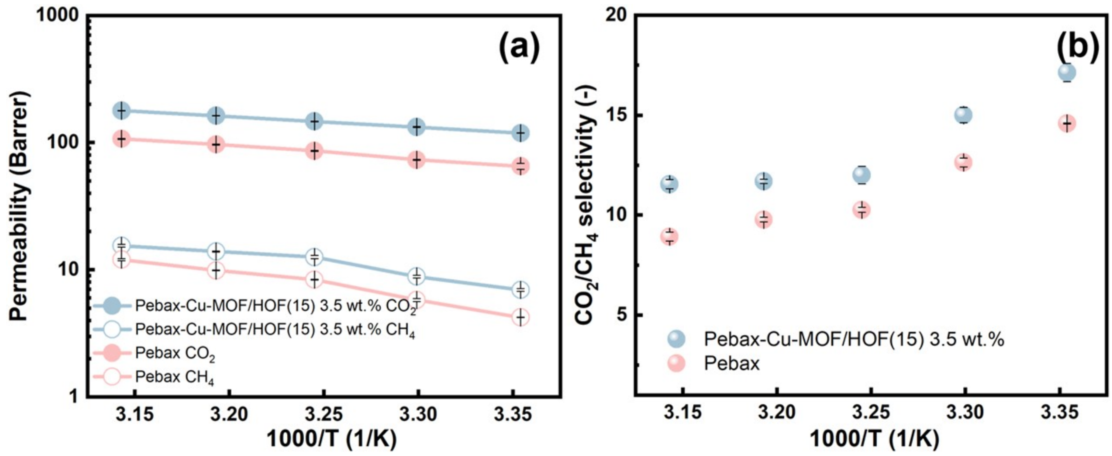

Fig. S15 CO_2/CH_4 separation performance of Pebax and Pebax-Cu-MOF/HOF(15) 3.5 wt.% MMM at 2 bar, different temperatures, gas permeability (a), and CO_2/CH_4 selectivity (b).

17. Long-term stability

The long-term stability of CO_2/CH_4 separation of Pebax-Cu-MOF/HOF (15) 3.5 wt.% MMM was tested at 2 bar, 25 °C, and the results are shown in **Fig. S16a**. The test procedure was carried out continuously for 10 days, and the stabilization stage was selected and recorded and the results showed that Pebax-Cu-MOF/HOF (15) 3.5 wt.% MMM had excellent long-term stability of CO_2/CH_4 separation.

To highlight the long-term stability advantage of the prepared Pebax-Cu-MOF/HOF(15) 3.5 wt.% MMMs, we tested the CO_2/N_2 separation performance of the original MMMs at 2 bar, 25 °C, and the results are shown in **Fig. S16b**. The above Pebax-Cu-MOF/HOF(15) 3.5 wt.% MMMs has now been placed at ambient temperature (seasonally affected, room temperature varies from 5 °C-30 °C), and in an open environment for 92 days. Notably, its P_{CO_2} can still be maintained at about 110.0 Barrer and $\alpha^*_{CO_2/N_2}$ can be maintained at 70.00, which has good long-term stability.

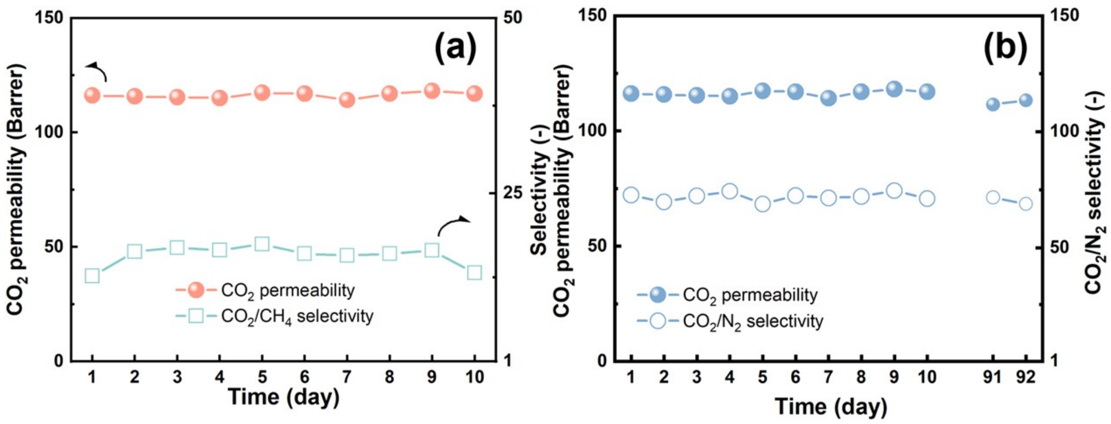

Fig. S16 Long-term stability Pebax-Cu-MOF/HOF(15) 3.5 wt.% MMM, at 2bar, 25 °C

18. Comparison of separation performance with others

Table S2. Comparison of gas separation performance of this work with other Pebax-functional MOFs MMMs

MMMs	Loading (wt.%)	T (°C)	Pressure (bar)	P_{CO_2} (Barrer)	$\alpha^*_{CO_2/N_2}$(-)	Ref
Pebax-ZIF-93-NH_2	5	25	4	84.18	65.51	
Pebax-ZIF-93-NH_2	10	25	4	84.52	65.28	[7]
Pebax-ZIF-93-NH_2	15	25	4	62.20	51.21	
Pebax-PSA@ZIF-8-NH2	10	25	1	99.86	59.49	[8]
Pebax-PDA-UiO-66	5	25	3	84.55	62.59	[9]
Pebax-CoZnZIF	5	35	1	106.7	47.55	
Pebax-PVP-CoZnZIF	5	35	1	99.14	41.33	[10]
Pebax-F127-CoZnZIF	5	35	1	109.9	48.49	
Pebax-[Bmim][PF_6]-ZIF-8	5	25	2	65.28	60.42	[11]
Pebax-[Bmim][PF_6]-ZIF-8	10	25	2	67.23	69.59	
Pebax-ZnCoZIF	10	30	12	90.84	68.70	[12]
Pebax-ZnCoZIF	12.5	30	12	86.02	66.10	
Pebax	-	25	2	65.22	49.73	
Pebax-Cu-MOF	2	25	2	82.08	59.12	
Pebax-Cu-MOF	3.5	25	2	79.25	59.43	
Pebax-Cu-MOF	5	25	2	79.67	60.49	
Pebax-Cu-MOF/HOF(10)	1	25	2	90.68	63.87	
Pebax-Cu-MOF/HOF(10)	2	25	2	98.84	69.40	
Pebax-Cu-MOF/HOF(10)	3.5	25	2	103.5	63.60	This work
Pebax-Cu-MOF/HOF(10)	5	25	2	93.77	68.06	
Pebax-Cu-MOF/HOF(15)	1	25	2	112.8	58.46	
Pebax-Cu-MOF/HOF(15)	2	25	2	128.5	63.72	
Pebax-Cu-MOF/HOF(15)	3.5	25	2	118.9	72.71	
Pebax-Cu-MOF/HOF(15)	3.5	25	4	122.3	70.32	
Pebax-Cu-MOF/HOF(15)	3.5	25	5	125.1	71.43	
Pebax-Cu-MOF/HOF(15)	3.5	25	6	129.2	75.33	

Reference

[1] J. Ma, J. Zhang, Y. Yuan, Y. Zhou, S. Cong, G. Xing, J. Wang, Z. Wang, HOF-21 nanofillers incorporated mixed matrix membranes for high-performance N2/CH4 separation, J. Membr. Sci., 677 (2023) 121626.

[2] Z. Bao, D. Xie, G. Chang, H. Wu, L. Li, W. Zhou, H. Wang, Z. Zhang, H. Xing, Q. Yang, M.J. Zaworotko, Q. Ren, B. Chen, Fine Tuning and Specific Binding Sites with a Porous Hydrogen-Bonded Metal-Complex Framework for Gas Selective Separations, J. Am. Chem. Soc., 140 (2018) 4596-4603.

[3] J. Wang, Y. Mao, R. Zhang, Y. Zeng, C. Li, B. Zhang, J. Zhu, J. Ji, D. Liu, R. Gao, Y. Ma, In Situ

Assembly of Hydrogen-Bonded Organic Framework on Metal–Organic Framework: An Effective Strategy for Constructing Core–Shell Hybrid Photocatalyst, Adv. Sci., 9 (2022) 2204036.

[4] W. Zhu, L. Wang, H. Cao, R. Guo, C. Wang, Introducing defect-engineering 2D layered MOF nanosheets into Pebax matrix for CO2/CH4 separation, J. Membr. Sci., 669 (2023) 121305.

[5] C. Zhang, P. Bei, H. Liu, X. Zhao, M. Shi, X. Jing, Z. Li, H. Yao, Preparation of M2070-UiO-66-OH@[BMim][PF6]/Pebax mixed matrix membranes and CO2 separation, Polymer Bulletin, (2025).

[6] D. Peng, S. Wang, Z. Tian, X. Wu, Y. Wu, H. Wu, Q. Xin, J. Chen, X. Cao, Z. Jiang, Facilitated transport membranes by incorporating graphene nanosheets with high zinc ion loading for enhanced CO2 separation, J. Membr. Sci., 522 (2017) 351-362.

[7] Y. Ding, H. Wang, M. Yu, W. Zheng, X. Ruan, X. Li, Y. Xi, Y. Dai, H. Liu, G. He, Amine group graft ZIF-93 to create gas storage space to improve the gas separation performance of Pebax-1657 MMMs, Sep. Purif. Technol., 309 (2023) 122949.

[8] R. Ding, Z. Li, Y. Dai, X. Li, X. Ruan, J. Gao, W. Zheng, G. He, Boosting the CO_2/N_2 selectivity of MMMs by vesicle shaped ZIF-8 with high amino content, Sep. Purif. Technol., 298 (2022) 121594.

[9] W. Zheng, D. Wang, X. Ruan, Y. Dai, X. Yan, X. Zhang, X. Li, X. Jiang, G. He, Pore engineering of MOFs through in-situ polymerization of dopamine into the cages to boost gas selective screening of mixed-matrix membranes, J. Membr. Sci., 661 (2022) 120882.

[10] R. Jayachitra, A. Prasannan, J.N. Jebaranjitham, S.-Y. Chen, R. Damastuti, P.-D. Hong, Facile synthesis of inherently MOF-integrated Pebax catalytic membrane for selective CO2 separation and photocatalytic degradation, Sep. Purif. Technol., 364 (2025) 132347.

[11] Z. Guo, W. Zheng, X. Yan, Y. Dai, X. Ruan, X. Yang, X. Li, N. Zhang, G. He, Ionic liquid tuning nanocage size of MOFs through a two-step adsorption/infiltration strategy for enhanced gas screening of mixed-matrix membranes, J. Membr. Sci., 605 (2020) 118101.

[12] M. Ghadiri, A. Aroujalian, F. Pazani, P. Salimi, Tailoring filler/gas vs. filler/polymer interactions via optimizing Co/Zn ratio in bimetallic ZIFs and decorating on GO nanosheets for enhanced CO_2 separation, Sep. Purif. Technol., 330 (2024) 125315.